Published in final edited form as:

Curr Biol. 2017 September 11; 27(17): 2569–2578.e4. doi:10.1016/j.cub.2017.07.013.

BORC regulates the axonal transport of synaptic vesicle precursors by activating ARL-8

Shinsuke Niwa[#,1,4], **Li Tao**[2,4], **Sharon Y. Lu**[2,4], **Gerald M. Liew**[3], **Wei Feng**[5], **Maxence V. Nachury**[#,3], and **Kang Shen**[#,2,5]

[1]Frontier Research Institute for Interdisciplinary Sciences and Graduate School of Life Sciences, Tohoku University, Aramaki Aza Aoba 6-3, Aoba-ku, Sendai, Miyagi 980-8578, Japan

[2]Howard Hughes Medical Institute, Department of Biology, Stanford University, 385 Serra Mall, Stanford, CA 94305, USA

[3]Department of Molecular and Cellular Physiology, Stanford University School of Medicine, 279 Campus Drive, Stanford, CA 94305, USA

[5]National Laboratory of Biomacromolecules, Institute of Biophysics, Chinese Academy of Sciences, 15 Datun Road, Chaoyang District, Beijing 100101, China

Summary

Axonal transport of synaptic vesicle precursors (SVPs) is essential for synapse development and function. The conserved ARF-like small GTPase ARL-8 is localized to SVPs and directly activates UNC-104/KIF1A, the axonal-transport kinesin for SVPs in *C. elegans*. It is not clear how ARL-8 is activated in this process. Here we show that part of the BLOC-1 related complex (BORC), previously shown to regulate lysosomal transport, is required to recruit and activate ARL-8 on SVPs. We found mutations in six BORC subunits-- *blos-1*/BLOS1, *blos-2*/BLOS2, *snpn-1*/Snapin, *sam-4*/Myrlysin, *blos-7*/Lyspersin and *blos-9*/MEF2BNB cause defects in axonal transport of SVPs, leading to ectopic accumulation of synaptic vesicles in the proximal axon. This phenotype is suppressed by constitutively active *arl-8* or *unc-104* mutants. Furthermore, SAM-4/Myrlysin, a subunit of BORC, promotes the GDP to GTP exchange of ARL-8 *in vitro* and recruits ARL-8 onto SVPs *in vivo*. Thus, BORC regulates the axonal transport of synaptic materials and synapse formation by controlling the nucleotide state of ARL-8. Interestingly, the other two subunits of BORC essential for lysosomal transport, *kxd-1*/KXD1 and *blos-8*/Diaskedin, are not required for the SVP transport, suggesting distinct subunit requirements for lysosomal and SVP trafficking.

[#]Corresponding authors shinsuke.niwa.c8@tohoku.ac.jp, nachury@stanford.edu and kangshen@stanford.edu (Lead Contact).
[4]these authors contribute equally

Author Contributions: Conceptualization, S.N. and K.S.; Investigation, S.N., L.T., S.Y.L., G.M.L., and M.V.N.; Resources, S.N., W.F., M.V.N. and K.S.; Writing, S.N., L.T., S.Y.L., M.V.N. and K.S.; Supervision, M.V.N. and K.S.; Funding Acquisition, S.N. and K.S.

Introduction

Axonal transport plays critical roles in neuronal development and morphogenesis [1, 2], and defects in axonal transport lead to many neuronal diseases [3-7]. Axonal transport of synaptic materials, including synaptic vesicle proteins, is essential for synapse formation and determines the location of synapses [8]. Synaptic vesicle proteins are produced and packaged into synaptic vesicle precursors (SVPs) in the cell body. SVPs are then transported to the synaptic terminal by a molecular motor UNC-104/KIF1A belonging to kinesin-3 family [9, 10]. UNC-104/KIF1A is functionally conserved among higher eukaryotes [11-13]. The activity of UNC-104 regulates the size and density of synapses *in vivo* and is controlled by an autoinhibitory mechanism [14, 15].

ARL-8, a conserved Arf-like small GTPase, activates the axonal transport of SVPs by unlocking the autoinhibition of UNC-104 [14]. ARL-8 directly binds to the stalk region of UNC-104 in a GTP-dependent manner [16, 17]. In *arl-8* loss-of-function mutants in *C. elegans*, synaptic vesicles (SVs) ectopically accumulate at proximal sites along the axon due to insufficient activation of UNC-104 [17]. Consistent with this model, the *arl-8* synaptic phenotype is suppressed by gain-of-function mutations in *unc-104* [14]. The vertebrate orthologs, ARL8A and ARL8B, have been implicated in trafficking and maturation of lysosomes [18]. In particular, ARL8B localizes to lysosomes and couples lysosomes to KIF5B (kinesin-1) through direct interactions to an adaptor protein SKIP [19]. This coupling enables lysosomes to be transported towards the cell periphery where microtubules plus ends are enriched [19].

The lysosomal localization of ARL8B is dependent on a 8-subunit protein complex, the biogenesis of the lysosome related organelle complex 1 (BLOC-1) related complex (BORC) [20]. Knockdown of individual BORC subunits in HeLa cells causes ARL8B to become diffusely localized to the cytoplasm, leading to juxtanuclear clustering of lysosomes. BORC is composed of eight conserved proteins, including BLOS1, BLOS2 and Snapin, which are components of BLOC-1 as well [21]. Another subunit of BORC, LOH12CR1/Myrlysin, is the ortholog of the *C. elegans* protein SAM-4 [20]. A recent study showed that SAM-4 regulates the UNC-104-mediated axonal transport of SVPs in *C. elegans* touch receptor neurons [22]. In *sam-4* loss-of-function mutants, synaptic markers are largely absent from the presynaptic terminals and ectopically localized to axonal shafts and the cell body. In addition, gain-of-function mutations in *unc-104* suppress the *sam-4* phenotype, suggesting that SAM-4, like ARL-8, might be required to fully activate UNC-104. Nevertheless, the relationship between SAM-4 and ARL-8 in the axonal transport of SVPs has not been elucidated. Moreover, the involvement of other BORC subunits in SVP transport has not been investigated. We found here that SAM-4 might function as a GEF for ARL-8 in the axonal transport of SVPs. We further presented genetic evidence that some but not all BORC subunits are indispensable for the axonal transport of SVPs *in vivo*.

Results

sam-4 and *arl-8* function in the same genetic pathway

We visualized synapses in the DA9 neuron by the DA9-specific expression of the synaptic marker RAB-3 fused with green fluorescent protein (GFP) (*Pitr-1::gfp::rab-3*) as described previously (Figures 1A and 1B) [23]. In wild-type animals, synapses form in a specific region along the dorsal axon, leaving the ventral axon, which is the most proximal part of the axon, the commissure, and the proximal dorsal axon devoid of synapses [23, 24]. We have shown that *Pitr-1::gfp::rab-3* can reliably visualize the localization of endogenous synapses in DA9 by analyzing the colocalization with other SV and active zone markers as well as via electron microscopy validation [14, 16, 17, 23, 25]. We also tested the localization of a late endosome marker, RAB-7, and a lysosome marker, LAAT-1, in DA9 (Figures S1A and S1B). GFP::RAB-7 is localized to both the cell body and the axon, but it is less enriched in synapses than GFP::RAB-3. On the other hand, the lysosomal marker LAAT-1 is exclusively localized to the cell body. These localization patterns are distinct from that of the synaptic vesicle markers such as *rab-3* and *snb-1* [16].

Using *Pitr-1::gfp::rab-3*, we have shown that the synapse pattern is disrupted in several *arl-8* mutant alleles [17]. As both *sam-4* and *arl-8* showed genetic interactions with *unc-104* and are essential for the axonal transport of SVPs [14, 16, 22], we genetically investigated the relationship between *sam-4* and *arl-8* in the axonal transport of SVPs. To investigate if *sam-4* is required for the synapse pattern, we examined a deletion allele of *sam-4*, *tm3828* using the *Pitr-1::gfp::rab-3* marker. Indeed, GFP::RAB-3 were mislocalized proximally in the *sam-4(tm3828)* animals (Figure 1C). This phenotype mimicked that of a weak loss-of-function allele of *arl-8, tm2388*, in which the 3′ UTR is deleted (Figure 1D). To test the genetic interaction between *arl-8* and *sam-4*, we examined double mutants. For these experiments we used a previously characterized, strong loss-of-function allele of *arl-8, wy271*, in which a part of the promoter and the start codon are deleted [17]. DA9 synapses were strongly mislocalized to the proximal axon and commissure in *arl-8(wy271)* (Figure 1E). In *arl-8(wy271)*; *sam-4(tm3828)* double mutants, the synapse distribution appeared to be indistinguishable from that of the *arl-8(wy271)* single mutant (Figures 1F and G). To quantitatively assess this phenotype, we measured the number of mis-accumulated GFP::RAB-3 puncta in the commissure and the length of the asynaptic region in the dorsal axon. These measurements showed that the double mutant was indeed similar to the *arl-8(wy271)* single mutant, suggesting that *arl-8* and *sam-4* function in the same genetic pathway (Figures 1H and I).

sam-4 acts upstream of *arl-8* to regulate axonal transport of SVPs

We have shown that ARL-8 activates UNC-104 to promote the axonal transport of SVPs [14, 16]. This is supported by the result that *arl-8(wy271)* could be rescued by the overexpression of wild-type UNC-104 or mutations that cause constitutive activation of UNC-104 [14, 16]. To understand the hierarchical relationships among *sam-4*, *arl-8* and *unc-104*, we used a cell-specific promoter to overexpress each factor individually in the DA9 neuron of mutant animals. Overexpression of *sam-4*, *arl-8* or *unc-104* cDNA under the cell-specific promoter (mig-13 promoter) in the *sam-4* mutant background rescued the DA9 synapse pattern to the

wild-type distribution (Figure 2A-D). In contrast, the *sam-4(tm3828)* mutant could not be rescued when *sam-4* cDNA is expressed in hypodermal cells or in the neighboring DB neurons, suggesting that *sam-4* functions cell-autonomously (Figure S2A-F). Unlike *unc-104*, overexpression of *unc-116* cDNA, the only kinesin-1 motor in *C. elegans*, could not restore SV distribution in the DA9 neuron in the *sam-4* mutant (Figure S2G-I). These results suggest that *sam-4* might function upstream of both *arl-8* and *unc-104*, and that SAM-4 functions cell-autonomously to regulate synapse pattern. Next, we tested whether or not *arl-8(wy271)* could be rescued by the expression of the wild-type *sam-4*, *arl-8* or *unc-104* gene. While overexpression of either wild-type *arl-8* or *unc-104* cDNA rescued the *arl-8(wy271)* mutant, overexpression of wild-type *sam-4* cDNA did not restore the ectopic synapses in the *arl-8(wy271)* mutant (Figure 2E-H). We confirmed these observations by measuring the number of ectopic GFP::RAB-3 puncta in the commissure and the length of the dorsal asynaptic region (Figure 2I and J). Finally, we crossed these three transgenes into the *unc-104(e1265)* mutant, which is a strong loss-of-function allele. The *unc-104(e1265)* mutant shows SV mis-localization to the cell body and the dendrite in DA9 [9, 25]. While overexpression of *unc-104* cDNA rescued the SV mis-localization as expected, the expression of neither wild-type *sam-4* nor *arl-8* cDNA rescued the *unc-104(e1265)* mutant (Figure S2J-M). Collectively, these data show a hierarchal relationship among *sam-4, arl-8* and *unc-104* where *sam-4* functions upstream of both *arl-8* and *unc-104*.

SAM-4 is required for the recruitment of ARL-8 to SVPs

Our previous results showed that ARL-8 is localized to SVPs during SVP trafficking [17]. Since *sam-4* functions upstream of *arl-8*, we asked if SAM-4 is required for the recruitment of ARL-8 onto SVPs. We co-expressed ARL-8::YFP and mCherry::RAB-3 in DA9 and recorded vesicle trafficking events in the ventral axon (Figure 1A). Consistent with published results [22], we could detect ARL-8::YFP on almost all the RAB-3-positive anterograde mobile SVPs in wild-type axons (Figures 3A and B). The percentage of these mobile SVPs that were ARL-8-positive was drastically reduced (median percentages were 100% and 0 % in *wild type* and *sam-4*, respectively), although RAB-3-positive anterograde mobile SVPs were still observed in the *sam-4(tm3828)* mutant (Figures 3A and B). This data indicates that, instead of localizing to mobile SVPs, ARL-8::YFP is mostly diffusely localized to the axoplasm. This result suggests that ARL-8 is recruited to SVPs by SAM-4. SAM-4 itself is also present on many RAB-3-positive anterograde mobile SVPs (Figure S3A-B and [22])

Given that SAM-4 is essential to recruit ARL-8, which is required for efficient SVP transport, onto SVPs, we anticipated that the SVPs in the *sam-4* mutant would be transported abnormally as in the *arl-8(wy271)* mutant to result in a steady state phenotype of SV proximal mis-accumulation. To test this, we directly observed SVP transport dynamics in the *sam-4(tm3828)* and *arl-8(wy271)* mutants. The speed of axonal transport is not affected in the *arl-8(wy271)* mutant [14]. Similarly, the speed of anterograde axonal transport in the *sam-4(tm3828)* mutant was comparable to *wild type* (1.51 ± 0.31 μm/sec in *wild type* and 1.62 ± 0.24 μm/sec in *sam-4*, n = 50 vesicles, statistically not significant, t-test). The speed of retrograde axonal transport was not affected, either (2.33 ± 0.21 μm/sec in *wt*, 2.21 ± 0.13 mm/sec in *sam-4*, n = 50 vesicles, not significant, t-test). In addition, we

compared the number of moving vesicles, dissociation rate and capture rate as described previously [16]. The numbers of anterogradely and retrogradely moving vesicles as well as the dissociation rate of stationary SVPs were both significantly decreased in the *sam-4(tm3828)* mutant compared to *wild type* (Figure 3C and 3D). Both *sam-4* phenotypes are similar to but weaker than the *arl-8(wy271)* mutant, consistent with the steady state axonal accumulation phenotype being weaker in the *sam-4* mutant compared to the *arl-8(wy271)* mutant (Figure 3C and D). In contrast, the capture rate was not affected, which is similar to the *arl-8(wy271)* mutant as well [16] (Figure 3E). These phenotypic similarity of *sam-4* with *arl-8* and genetic interactions argue strongly that SAM-4 is an upstream regulator of ARL-8 in SVP transport.

The *arl-8* mutant with the GTP-state mimicking mutation suppresses *sam-4* phenotypes

Three lines of published evidence support the notion that ARL-8's function in activating UNC-104 is dependent on its nucleotide state. First, unlike the wild type ARL-8 which exhibits membrane binding, ARL-8(T34N), a mutant ARL-8 that mimics the GDP-bound state, is diffusely localized to the axoplasm [17]. Second, two mutant forms of ARL-8, ARL-8(Q75L) and ARL-8(D133N), which mimic GTP-bound ARL-8, can rescue the *arl-8(wy271)* mutant while ARL-8(T34N) cannot [17]. Third, ARL-8(Q75L) and ARL-8(D133N), but not ARL-8(T34N), bind to the stalk domain of UNC-104 [14, 16]. These previous findings and data presented here suggested that *sam-4* might regulate the nucleotide-binding state of *arl-8*. If SAM-4 promotes the GTP bound state of ARL-8, a constitutively active ARL-8 might no longer required SAM-4. To test whether the GTP-locked ARL-8 bypasses the need for SAM-4, we examined the *arl-8(jpn1); sam-4(tm3828)* double mutants. The *jpn1* allele was generated by CRISPR/Cas9 and contains the D133N mutation in the endogenous locus [14]. In this mutant, we have shown that the size and density of synapses are reduced, likening the effect caused by overexpressing wild-type ARL-8 [14, 16]. The mis-localization of synaptic vesicles was significantly reduced in the *sam-4(tm3828)*; *arl-8(jpn1)* double mutants compared to the *sam-4(tm3828)* single mutants (Figure 4A-C). While the *sam-4(tm3828)* mutants did not have significantly more mislocalized puncta in the commissure, the length of the asynaptic region was significantly shorter than *wild type* (Figure 4D and E). The length of the asynaptic region was recovered to wild-type level in the double mutant (Figure 4E; The median lengths of *wild type*, *sam-4(tm3828)* and *sam-4(tm3828); arl-8(jpn1)* were 27.7 mm, 3.0 mm and 24.2 mm, respectively, N = 20 animals). This genetic interaction means that SAM-4 is not required for the axonal transport of SVPs when ARL-8 is locked in the GTP form, suggesting that SAM-4 regulates the GTP state of ARL-8.

SAM-4 exhibits ARL-8 GEF activity *in vitro*

These genetic and cell biological data suggest that SAM-4 might serve as a guanine nucleotide exchange factor (GEF) for ARL-8. To directly test this hypothesis, we performed *in vitro* biochemical assays to determine whether SAM-4 physically interacts with ARL-8 and whether SAM-4 exhibits GEF activity toward ARL-8. We first expressed GFP-tagged ARL-8 together with Myc-tagged SAM-4 in HEK293 cells (Figure 5A). We found that SAM-4 can be co-immunoprecipitated with GFP-ARL-8, suggesting that SAM-4 and ARL-8 physically interact with each other. To test whether the interaction between ARL-8

and SAM-4 is direct and regulated by the nucleotide state of ARL-8, we conducted GST-capture assays with purified recombinant proteins using various buffers to mimic the different nucleotide states of ARL-8. We found that GST-ARL-8 captured SAM-4 only in the presence of EDTA (Figure 5B), which mimics nucleotide-free ARL-8. However, SAM-4 did not bind to ARL-8-GTP, ARL-8-GDP.AlF_x^- (mimic for the transition state of hydrolysis) or ARL-8-GDP. These data suggest that SAM-4 might be a GEF for ARL-8 as previous studies showed that GEFs strongly bind to the nucleotide-free state of the GTPases in the transition between the GDP-bound and GTP-bound states and have weaker binding affinity for the GDP-bound and GTP-bound states [26].

To directly test the hypothesis that SAM-4 is part of the ARL-8 GEF, we loaded purified ARL-8 with radioactive GDP and monitored the release of GDP from ARL-8 in the presence or absence of purified SAM-4 and excess cold GTP. In the absence of SAM-4, the GDP dissociated with a half life ($t_{1/2}$) of 13.0 ± 1.0 min, whereas in the presence of SAM-4, the GDP dissociation is modestly but significantly sped up ($t_{1/2}$ = 8.1 ± 1.1 min, Mean ± standard error of means, n = 3, p = 0.0003, paired t-test). SAM-4's GEF activity is specific towards ARL-8 because the addition of SAM-4 did not increase the GDP dissociation rate of SAR1A, another small GTPase involved in membrane trafficking (Figure S4). Taken together, these biochemical and genetic data argue that SAM-4 functions as part of the GEF for ARL-8 to promote SVP transport.

blos-9 regulates the axonal transport of SVPs together with *sam-4*

To further understand other factors that are required for ARL-8 activation, we performed forward genetic screens to isolate mutants in which ARL-8::YFP detaches from vesicles. We screened 600 haploid genomes and isolated a mutant, *jpn2*, in which ARL-8::YFP was more cytosolic and diffused than in *wild type* (Figure S5A-C). Through whole genome sequencing analysis, we identified a stop codon mutation in the *blos-9* gene (Figure S5D). *blos-9* encodes the *C. elegans* ortholog of MEF2BNB/BORC subunit 8, which is one of the eight subunits of BORC [20]. In *blos-9(jpn2)*, GFP::RAB-3 puncta were proximally mis-localized in DA9 (Figures 6A, 6B, S5E and S5F), suggesting that *blos-9* regulates the axonal transport of SVPs. Expression of *blos-9* genomic DNA in DA9 (with a mig-13 promoter), but not muscle cells (with a myo-3 promoter) or hypodermal cells (with a dpy-7 promoter), rescued the synaptic distribution phenotype in *blos-9(jpn2)*, suggesting that BLOS-9 functions cell-autonomously in DA9 (Figures 6C, S5G and S5H). Next, we tested whether *blos-9* and *sam-4* function in the same genetic pathway by examining the double mutants. The *blos-9(jpn2); sam-4(tm3828)* double mutants showed similar but not stronger synaptic phenotypes compared to the *blos-9(jpn2)* single mutant (Figures 6D,G,H and S6H,I,KM,N,O). Together, these evidence argue strongly that *blos-9* and *sam-4* work in the same genetic pathway in regulating the axonal transport of SVPs. Moreover, the *blos-9(jpn2)* mutant phenotype was suppressed by the gain-of-function mutants of *arl-8* or *unc-104* (Figure 6E-H) as the *sam-4* phenotype was (Figures 2 and 4 and [22]). Finally, we expressed BLOS-9::GFP in DA9 neuron and found that BLOS-9 co-localized with a synaptic vesicle marker, mCherry::RAB-3 (Figure 6I-L), suggesting that BLOS-9 is localized on SVs like SAM-4 [22].

BORC regulates the axonal transport of SVPs

To further test the involvement of other BORC subunits in axonal transport, we generated deletion mutants of *blos-2, blos-7 and blos-8* by CRISPR/Cas9 (Figure S6A) and examined the existing deletion mutants *blos-1(ok3707)*, *kxd-1(tm6384)* and *snpn-1(tm1892)*. While no defect was found in the *kxd-1(tm6384)* and *blos-8(wy1160)* deletion mutants, the SV distribution in the *blos-1(ok3707)*, *snpn-1(tm1892)*, *blos-2(jpn17)* and *blos-7(tm1159)* mutants showed similar proximal mis-accumulation as in the *sam-4(tm3828)* and *blos-9(jpn2)* mutants (Figures 7A-I). These results suggest that *blos-1*/BLOS1, *blos-2*/BLOS2, *snpn-1*/Snapin, *sam-4*/Myrlysin, *blos-7*/Lyspersin and *blos-9*/MEF2BNB are required for the SVP transport, but *kxd-1*/KXD1 and *blos-8*/Diaskedin are not. Interestingly, KXD-1::mRuby co-localized with SNB-1::YFP at the synapses, suggesting that KXD-1 may be on mature SVs or SVPs to serve a function distinct from SVP trafficking (Figure S7). To further confirm that the BORC complex subunits function in the same genetic pathway, we created two more double mutants between *sam-4* and other BORC subunits. The *blos-1*; *sam-4* and *snpn-1*; *sam-4* double mutants showed similar SV mis-localization as the *sam-4* single mutants, consistent with the notion that SAM-4 and other BORC subunits function in the same genetic pathway in regulating the axonal transport of SVPs (Figures S6B-O).

To ask if BORC subunits are required to recruit ARL-8 onto SVPs, we performed time-lapse imaging experiments to observe ARL-8::YFP localization on mobile SVPs in the DA9 ventral axon of BORC mutants. Indeed, ARL-8::YFP is largely absent from the mobile mCherry::RAB-3 SVPs and instead diffusely localized in the axoplasm in *blos-1*, *blos-9* and *snpn-1* mutants (Figure 7J and K; the median percentage of ARL-8-positive anterograde RAB-3 events was 0% in all mutants, compared to 100% in *wild type*). To address whether the transport of SVPs is affected, we examined the dynamic parameters of RAB-3-positive SVP puncta in the *blos-1(ok3707)* and *blos-2(jpn17)* mutants. We found that both mutants showed reduced frequency of moving puncta and dissociation of stable puncta in both anterograde and retrograde directions compared to *wild type* (Figures 7L, 7M and S6P). These phenotypes are similar to those found in the *sam-4(tm3828)* mutant (Figure 3). Moreover, to understand if BORC subunits also play a role together to regulate other aspects besides the axonal transport of SVs, we examined the overall fitness of the BORC mutants by counting their brood sizes. The single mutants *sam-4*, *blos-1, snpn-1* or *blos-9* have brood sizes similar to *wild type* (Figure S6Q-S). The brood size of *sam-4; blos-9* double mutants does not differ from single mutants or *wild type* (Figure S6S). In contrast, the *sam-4; blos-1* and *sam-4; snpn-1* double mutants have significantly reduced brood sizes compared to single mutants and *wild type* (Figure S6Q-R). Given that *blos-9* is a BORC-specific subunit whereas *blos-1* and *snpn-1* are shared between the BORC and the BLOC-1 complex, these brood size data suggest that *sam-4* regulates brood sizes through a pathway parallel to the regulation of SVPs. Together, these results suggest that multiple BORC subunits are essential to recruit ARL-8 onto SVPs.

Discussion

BORC regulates ARL-8- and UNC-104-dependent anterograde axonal transport of SVPs

BORC is a multi-subunit protein complex that was originally shown to regulate lysosomal transport through recruiting ARL-8 onto lysosomes in HeLa cells [20].All eight subunits of BORC are conserved from *C. elegans* to human, suggesting that it plays important functions in cell biology. Several critical questions regarding BORC remain unanswered. First, does BORC specifically regulate lysosomal transport or does it also regulate other organelles? Second, what is the function of BORC *in vivo*? Third, if BORC regulates ARL-8, what is the biochemical mechanism for this regulation? Here, we presented genetic, biochemical and cell biological data suggesting that part of BORC regulates the axonal transport of SVPs by activating ARL-8 and UNC-104 *in vivo*. Our biochemical data suggest that SAM-4, a BORC subunit, acts as a GEF for ARL-8 to recruit ARL-8 onto SVPs.

Axonal transport of SVPs is fundamental to synaptic development and functions. Our previous works have shown that ARL-8 is a small GTPase on SVPs and that ARL-8 activates UNC-104/KIF1A-dependent axonal transport of SVPs by relieving the autoinhibition of UNC-104 [14]. In addition, one published work showed that SAM-4/Myrlysin plays important roles in synapse formation in the touch receptor neurons of *C. elegans*[22]. Through genetic analysis, they showed that *sam-4* genetically interacts with *unc-104* to regulate axonal trafficking of SVPs. However, the molecular mechanism is largely unknown. Although both *sam-4* and *arl-8* could be suppressed by the gain-of-function *unc-104* mutations, no functional interactions between SAM-4 and ARL-8 had been reported. The genetic experiments presented in this paper argue strongly that SAM-4, along with other BORC subunits, is the upstream regulator of ARL-8 in the axonal transport of SVPs.

Although most of the BORC complex function in the same genetic pathway to regulate the axonal transport of SVPs, our brood size data suggested that some subunits may also have other functions in parallel with *sam-4*, at least in regulating the number of progeny in *C. elegans*. Consistent with this notion, SNPN-1/Snapin and BLOS-1/BLOS1 subunits are shared by a different protein complex called BLOC-1 which is essential for the biogenesis of lysosome-related organelles [20, 27].

Snapin is one of the subunits of BORC. In Snapin knockout mice, synaptic late endosomes are defective [28]. The authors showed that Snapin directly interacts with dynein intermediate chain and suggested that Snapin activates the retrograde transport of synaptic endosomes [29]. This function of Snapin is likely to also require dysbindin, a component of BLOC-1, but not BORC. It is interesting to note that retrograde trafficking of SVPs is also reduced in *arl-8* mutants [16]. Whether this defect directly involves BORC or BLOC-1 remains to be tested.

BORC is a GEF for ARL-8

While the link between ARL-8 and BORC in lysosomal trafficking is well established based on cell biological experiments, the biochemical mechanism of how BORC regulates ARL-8 remains unclear [20]. Four lines of evidence presented here are consistent with the notion

that BORC is a GEF for ARL-8. First, ARL-8 is more cytoplasmic and much less localized to SVPs in the BORC mutants (Figures 3A-B and 7J-K). Arf-like small GTPases generally bind to membranes or protein complexes when they are converted to the GTP form [30, 31]. Thus, it is plausible that cytosolic ARL-8 is mostly in the GDP form in the BORC mutants. Consistent with this possibility, we showed that the GDP-form mimicking ARL-8 (T34N) shows a diffuse cytosolic pattern, while the GTP-form mimicking ARL-8 (Q75L) form shows a membrane localization pattern [17]. Second, *arl-8(jpn1)* suppresses the SV mis-localization observed in the BORC mutants. *arl-8(jpn1)* contains a point mutation that locks ARL-8 in the GTP state [14]. The *sam-4(tm3828)*; *arl-8(jpn1)* and *blos-9(jpn2)*; *arl-8(jpn1)* phenotypes are similar to the *arl-8(jpn1)* alone, suggesting that *arl-8* is epistatic to the BORC genes. This is consistent with the notion that BORC is required for ARL-8 activation and recruitment to membranes (Figures 4 and 6E; [14]). Third, our biochemical experiments showed that purified SAM-4 and ARL-8 could bind directly to each other. Interestingly, the binding is detected only when ARL-8 is in a nucleotide-free state. The binding was not detected when ARL-8 was loaded with GDP, GTPγS or AlF_x^- (Figure 5B). These results are consistent with the notion that GEFs bind preferentially to the nucleotide-free GTPases [26]. Lastly, a GEF assay directly showed that SAM-4 sped up the dissociation of GDP from ARL-8 (Figure 5C). While BORC is a multi-subunit complex, our data suggest that SAM-4 directly interacts with ARL-8 and has a modest GEF activity for ARL-8 *in vitro*. Since genetic data showed that not only SAM-4 but also other BORC subunits are essential for the axonal transport of SVPs, it is likely that the entire BORC complex is required to reconstitute the maximal ARL-8 GEF activity *in vitro*. Comparison of the GEF activity between SAM-4 alone and entire BORC complex would be required to clarify this question.

The similarity and difference between SVP and lysosomal transport

Through an unbiased forward genetic screen, we identified BLOS-9/MEF2BNB to be important for ARL-8 membrane localization and SVP axonal transport (Figures 6 and S5A-D). However, MEF2BNB is a non-essential subunit of BORC for the lysosomal transport in HeLa cells [20]. In contrast, while KXD-1/KXD1 and BLOS-8/Diaskedin are dispensable for the axonal transport of SVPs (Figure 7A, 7B and 7G), both are required for lysosomal transport [20]. SAM-4/Myrlysin, BLOS-1/BLOS1, BLOS-2/BLOS2, SNPN-1/Snapin, and BLOS-7/Lyspersin are essential for both SVP and lysosomal transport. These genetic data suggest that there might be two kinds of BORC sub-complexes with distinct functions. Purification of BORC from lysosomal and SV fractions would be required to fully test this hypothesis.

While lysosomal transport depends on two motors, KIF5/UNC-116 (kinesin-1) and KIF1Bβ/UNC-104 (kinesin-3) [32], genetic data in *C. elegans* strongly suggest that the axonal transport of SVPs depends solely on UNC-104 (Figure S2G-I and [9, 10, 16, 33]). For lysosomal transport, KIF5 (kinesin-1) forms a complex with ARL-8 via SKIP, an adaptor protein that binds to both ARL-8 and KIF5 [34]. The GTP form of ARL8B binds to SKIP to recruit KIF5 onto the lysosomal membrane. Although a recent study has shown that this complex is essential for the axonal transport of lysosomes [35], we could not analyze the role of BORC in this phenomena in this study as mature lysosomes are largely absent in DA9 axons (Figure S1B).

In contrast, SKIP is not required for KIF1Bβ to transport lysosomes [32]. How KIF1Bβ binds to the lysosomal membrane remains elusive. KIF1Bβ is a kinesin-3 family member that is structurally and functionally similar to KIF1A. While KIF1A is a neuron specific isoform, KIF1Bβ is expressed in both neuronal and non-neuronal cells [11, 36]. For SVP transport, ARL-8 does not simply work as an adaptor for UNC-104/KIF1A/KIF1Bβ (kinesin-3). Instead, ARL-8 on SVPs directly binds to the stalk domain of UNC-104/KIF1A in a nucleotide-state dependent manner [14, 16]. This binding releases the autoinhibition of UNC-104/KIF1A and fully activates UNC-104/KIF1A [14]. How motors discriminate specific cargos remains an open question. It is possible that the difference in the BORC subunit composition on SVPs and lysosomes affects the motor specificity. Future experiments are needed to test this hypothesis.

Contact for Reagent and Resource Sharing

Further information and requests for resources and reagents should be directed to and will be fulfilled by the Lead Contact,Kang Shen (kangshen@stanford.edu).

Experimental Model and Subject Detail

Caenorhabditis elegans

Caenorhabditis elegans var Bristol was used as *wild type*. Young adult hermaphrodites were analyzed unless otherwise noted. Strains were maintained on lawns of Escherischia coli OP50 feeder on NGM (1.7% (w/v) agarose, 50mM NaCl, 0.25% (w/v) Peptone, 1 mM CaCl2, 5 mg/ml Cholesterol, 25 mM KH2PO4, 1 mM MgSO4) under standard conditions at 20°C. *arl-8(wy271), arl-8(jpn1), unc-104(wy873), wyIs85, wyIs86*, and *wyIs92* are described previously [14, 17, 23]. *arl-8(tm2388), sam-4(tm3828), snpn-1(tm1892)* and *kxd-1*(*tm6384)* were obtained from Japanese National BioResourse Project (Mitani lab, Japan). *blos-1*(*ok3707)* was obtained from CGC.

Methods Details

Transgenesis

To generate *wyIs546*, plasmids encoding *Podr-1::gfp* (co-injection marker), *Pitr-1::arl-8::yfp*, and *Pitr-1::mcherry::rab-3 were* co-injected into wild type worms as described [37]. Young adult worms were fixed on a dried agar pad and covered with Halocarbon oil 700 (Sigma-Aldrich, St. Lous, MO, USA). Plasmids were injected to gonads by glass needles under the standard differential interference contrast (DIC) microscope equipped with x40 or x63 lens (Leica microsystems, Wetzlar, Germany or Carl Zeiss, Jena, Germany) equipped with a micro minipulator (Narishige, Tokyo, Japan) and a microinjector Femtojet (Eppendorf, Hamburg, Germany). Worms were recovered and cultured at 20°C for 3 days. At the F1 generation, Podr-1::gfp-positive worms were picked up under the standard fluorescent dissection microscope (Nikon, Tokyo, Japan or Carl Zeiss). At the F2 generation, lines that have extrachromosomal arrays were selected. Insertion of the extra chromosomal array to the worm genome was performed by UV irradiation. L4 worms that have extrachromosomal arrays were irradiated by 300 J/m^2 UV light using UV cross linker. 3 days later, 100 F1 worms were picked up. At F2 generation, 5 worms were singled from each F1. Worms that

shows 100% transmission were selected and outcrossed with wild type at least 3 times. To generate *wyIs1075*, *Pmig-13::sam-4a::gfp*, *Pmig-13::tdTomato::rab-3*, and *Podr-1::gfp* were co-injected into wild type worms and genomic insertion was performed as described. To generate *wyEx4837*, plasmids encoding *Pmig-13::gfp::rab-7* and *Podr1::rfp* were co-injected into wild type worms. To generate *wyEx8985*, plasmids encoding *Pitr-1::laat-1::gfp* and *Podr-1::rfp* were co-injected into wild type worms. To generate *wyEx2339*, *Pitr-1::arl-8::yfp* and *Podr-1::gfp* were co-injected into wild type worms. To generate *wyEx9053*, *Pmig-13::kxd-1::mRuby* and *Podr-1::gfp* were co-injected into wild type worms. To generate *jpnEx37*, *Pitr-1::blos-9(genomic DNA)::gfp* and *Pmig-13::mcherry::rab-3* were co-injected to wild type worms.

Molecular biology

mig-13 promoter (DA9 promoter), *unc-104* promoter (pan-neuronal promoter), *arl-8* cDNA and *unc-104* cDNA were described previously [14, 16, 17, 23]. *sam-4*, *rab-3*, *rab-7*, and *kxd-1* cDNA were amplified by polymerase chain reaction (PCR) from worm cDNA obtained from N2 strain. *blos-9* and *laat-1* genomic DNA was amplified by PCR from N2 genomic DNA. PCR was performed using KOD-plus- high fidelity DNA polymerase (TOYOBO, Tokyo, Japan). These DNA fragments were assembled on the pSM vector (with GFP fusion, obtained from Cori Bargmann, Rockefeller University) or ΔpSM vector (without GFP fusion, obtained from Cori Bargmann).

Genome editing

blos-2(*jpn17*), *blos-7(wy1159)* and *blos-8(wy1160)* were generated by CRISPR/Cas9 asdescribed [38]. The target sequence for *blos-2* was 5′-CTGCCAATTGTCTGATATGTGG-3′. The sequence was inserted to pRB1017 vector (gift from Andrew Fire, addgene #59936). pDD162 (a gift from Bob Goldstein, addgene #47549) was used to express Cas9. pJA58 (a gift from Andrew Fire, addgene #59933) and the repair template single strand DNA (AF-ZF-827), that generate *dpy-10(cn64)* mutation, were used as a co-CRISPR marker. These vectors and oligonucleotide were injected to young adult worms as described above and *dpy* or *rol* mutants were picked up. The deletion was screened by PCR followed by MfeI treatment (Fig S6A). For genotyping, Takara Ex Taq was used as described in the manufacture's protocol (Takara, Tokyo, Japan). PCR primers for genotyping are following: 5′-aaatatttcgtgtcgagacctggtgc-3′ and 5′-acacgcaaacttcttgaaacgaacac-3′. Wild-type worms give 210 bp and 217 bp bands while *blos-2*(*jpn17*) worms give a 414 bp band.

For *blos-7(wy1159)*, two guide RNA sequences (without PAM) 5′-GAAAGAAGTGGCTGGGAAG-3′ and 5′-ATCAGAAGCGAGCCGGTGA-3′ were used. The deletion was ~1900 bp and confirmed by PCR (Fig S6A). Three primers 5′-CGCTGCTTGCCCACCGAATACATAA-3′, 5′-CATGTCCAATGTGCTACGCGAG TTTC-3′, and 5′- CAAATCGTCGACTACGAAGGACGTCTG -3′ were used for genotyping. Wild-type worms give ~380 bp while *blos-7(wy1059)* worms give a ~570 bp band.

For *blos-8(wy1160)*, Three guide RNAs were used. The sequences (without PAM) were following: 5′-GCACATTATCG ATTCCTGC-3′, 5′-TGAATTTGTAGAGGCCTGC-3′ and 5′ CGTCAAAACTACTACAGCG-3′. wy1160 contains a ~ 680 bp deletion that was confirmed by PCR (Fig S6A). The genotyping primer sequences are 5′-TTCCAGACCCTTCTCACAAGTGCAA-3′, 5′-CGCGAATACAAATTCCTGCGC AAGT-3′ and 5′-GCCCAAAGCGTGAATTTCATAGTGTGA-3. Wild-type worms give~ 380 bp while *blos-8(wy1060)* worms give a ~760bp band.

Recombinant Protein Expression and Purification

arl-8 cDNA was cloned into pGEX6P vectors (GE HealthCare, Little Chalfont, UK) with HPV3C-cleavable GST tags, and was expressed in BL21 cells. The membrane binding motif of ARL-8, the first 19 amino acids, was deleted in the biochemical experiments as described previously [14, 16]. GST-ARL-8 was purified on Glutathione Sepharose 4B (GE Healthcare Life Sciences, Pittsburgh, PA, USA) resin then subjected to size-exclusion chromatography for further purification and buffer change. ARL-8, which was used for the GEF assay, was purified using Glutathione Sepharose 4B (GE Healthcare) resin. Then, the Glutathione S-transferase (GST) tag was cleaved by incubation with HRV3C at 4°C overnight. SAM-4 was also expressed from derivatives of pGEX6P, and was purified the same way as ARL-8.

GST-Capture Assay

100 μg purified SAM-4 was mixed with 100 μg GST- ARL-8 or GST (control) in 250 to 300 μL HBS buffer (50 mM HEPES, pH 7.4, 150 mM NaCl, 1 mM $MgCl_2$) which containing either 1 mM GDP, 1 mM GTPγS, 20 μM EDTA, or 1 mM GDP/2 mM $AlCl_3$/20 mM NaF. Reactions were first incubated at 30°C for 1hour and then shift to 4°C for binding. 10 μL Glutathione Sepharose 4B beads were used for each reaction. After binding, proteins were eluted by HRV3C cleavage.

GEF assay

Binding of radiolabeled nucleotides to ARL-8 was measured by filter assays [39]. For each reaction, 0.1 μM of ARL-8ΔN19 was loaded with 2.25 μM [^{3}H] GDP in 1X loading buffer (50 mM HEPES, pH 7.0, 150 mM KOAc, 1 mM $Mg(OAc)_2$, 0.2 mg/mL BSA, 0.1% Triton X-100, and 1 mM DTT) at 32°C for 2 hours. After loading, the reactions were incubated on ice for cooling down. Exchange reaction was initiated by addition 0.5 mM GTP and 10 mM SAM-4 or GST(control) and incubated at 25 °C. Six time points were taken for the measurement. $t_{1/2}$ was calculated by fitting the data as a single exponential decay equation.

Fluorescent imaging

Time-lapse imaging of fluorescently tagged proteins in the DA9 ventral axon of live *C. elegans* was performed on an inverted Zeiss Axio Observer Z1 microscope equipped with a Plan-Apochromat 100x/1.4 objective, a Hamamatsu EM-CCD digital camera and a Yokogawa CSU-X1 spinning disk. Prior to movie acquisition, L4 worms grown at room temperature were anesthetized with 10mM levamisol for 10 minutes then transferred onto 5 % agarose pads with M9 buffer. For each movie, following 3.5 seconds of bleaching, 45 frames were acquired over ~30 seconds with an exposure time of 300 ms. ImageJ (NIH) was

used to generate straightened axons, which were inputted to Matlab to make kymographs. For steady state imaging of fluorescently tagged proteins in the DA9 neuron of live *C. elegans*, a 40x/1.4 objective was used. Prior to imaging, L4 worms grown at 20°C were mounted onto 5 % agarose pads with 1 mM levamisol in M9 buffer. ImageJ (NIH) was used to generate straightened axons, which contain the entire synaptic region and were aligned at the commissure bend on the right and stacked in rows with one axon in each row. An off-black background box is used for visual cleanliness as different axons were traced to different distances distally past the synaptic region.

Quantification and Statistical Analysis

A minimum of three independent biological replicates were performed for each experiment. For transgenic experiments, at least three independent transgenic lines were observed and results from one representative transgenic line was shown. Statistical analysis was performed using Microsoft Excel 2013 (Microsoft, Redmond, WA, USA) using Excel TOUKEI 2015 (BellCurve, Tokyo, Japan) in Figure 1, 2, 3C-E, 4, 5C, 6, S2 and S5 and GraphPad Prism (GraphPad Sofware Inc., La Jolla, CA, USA) for Figure 3B and 7, S3 and S6.

Student's t-test was used to compare axonal transport parameters (Figure 3C-E, 7L-M and S6P) as described [16], paired t-test was used to compare the amount of dissociated GDP in each time point (Figure 5C), Mann-Whitney test was used to compare the percentage of ARL-8-positive anterograde RAB-3 events in *wild type* (*wt*) and *sam-4(tm3828)* animals (Figure 3B), Kruskal–Wallis one-way ANOVA on ranks and Dunn's multiple comparisons test were used to compare the number of puncta mis-accumulated to the commissure and the length of the asynaptic region (Figure 1H-I, 2I-J, 4D-E, 6G-H, 7H-I, S2A-B, S5G-H, S6F-G, S6N-O). The number of samples and statistical methods were clearly described in the figure legend of each figure. Axonal transport parameters (Figure 3C-E, 7L-M and S6P) and the amount of dissociated GDP (Figure 5C) were shown as mean ± standard error of the mean (SEM). Each value and median were plotted by dot and bar to show the percentage of ARL-8-positive anterograde RAB-3 events in *wild type* (*wt*) and *sam-4(tm3828)* animals (Figure 3B) and the number of puncta mis-accumulated to the commissure and the length of the asynaptic region (Figure 1H-I, 2I-J, 4D-E, 6G-H, 7H-I, S2A-B, S5G-H, S6F-G, S6N-O). These were described in the figure legend of each panel as well. No statistical methods were used to predetermine the size of datasets. Asterisks indicate a significant difference between the results for indicated experimental conditions (*, $p < 0.05$; **, $p < 0.01$, ***, $p < 0.001$).

Supplementary Material

Refer to Web version on PubMed Central for supplementary material.

Acknowledgments

The authors wish to thank members in the Shen lab at Stanford University and in the Sugimoto lab at Tohoku University. This research was supported by the National Basic Research Program of China (2013CB910103), the Howard Hughes Medical Institute, and the National Institutes of Health (R01 NS048392) to K.S. This research was also supported by the JSPS KAKENHI (16H06536 and 17H05010) and the Tomizawa Jun-ichi and Keiko Fund of Molecular Biology Society of Japan for Young Scientists to S.N., National Institutes of Health (R01 GM089933) to M. V. N., the Stanford Graduate Fellowship to S.Y.L. and, the National Natural Science Foundation of China

(31428009) to W. F and K. S. Many strains were provided by the CGC, which is funded by the NIH Program (P40 OD010440). The authors declare that there is no conflict of interest regarding the publication of this work.

References

1. Hirokawa N, Noda Y, Tanaka Y, Niwa S. Kinesin superfamily motor proteins and intracellular transport. Nat Rev Mol Cell Biol. 2009; 10:682–696. [PubMed: 19773780]
2. Vale RD. The molecular motor toolbox for intracellular transport. Cell. 2003; 112:467–480. [PubMed: 12600311]
3. Holzbaur EL, Scherer SS. Microtubules, axonal transport, and neuropathy. N Engl J Med. 2011; 365:2330–2332. [PubMed: 22168648]
4. Morfini GA, Burns M, Binder LI, Kanaan NM, LaPointe N, Bosco DA, Brown RH, Brown H, Tiwari A, Hayward L, et al. Axonal transport defects in neurodegenerative diseases. J Neurosci. 2009; 29:12776–12786. [PubMed: 19828789]
5. Niwa S, Takahashi H, Hirokawa N. β-Tubulin mutations that cause severe neuropathies disrupt axonal transport. EMBO J. 2013; 32:1352–1364. [PubMed: 23503589]
6. Kevenaar JT, Bianchi S, van Spronsen M, Olieric N, Lipka J, Frias CP, Mikhaylova M, Harterink M, Keijzer N, Wulf PS, et al. Kinesin-Binding Protein Controls Microtubule Dynamics and Cargo Trafficking by Regulating Kinesin Motor Activity. Curr Biol. 2016; 26:849–861. [PubMed: 26948876]
7. Rivière JB, Ramalingam S, Lavastre V, Shekarabi M, Holbert S, Lafontaine J, Srour M, Merner N, Rochefort D, Hince P, et al. KIF1A, an axonal transporter of synaptic vesicles, is mutated in hereditary sensory and autonomic neuropathy type 2. Am J Hum Genet. 2011; 89:219–230. [PubMed: 21820098]
8. Maeder CI, Shen K, Hoogenraad CC. Axon and dendritic trafficking. Curr Opin Neurobiol. 2014; 27:165–170. [PubMed: 24762653]
9. Hall DH, Hedgecock EM. Kinesin-related gene unc-104 is required for axonal transport of synaptic vesicles in C. elegans. Cell. 1991; 65:837–847. [PubMed: 1710172]
10. Otsuka AJ, Jeyaprakash A, García-Añoveros J, Tang LZ, Fisk G, Hartshorne T, Franco R, Born T. The C. elegans unc-104 gene encodes a putative kinesin heavy chain-like protein. Neuron. 1991; 6:113–122. [PubMed: 1846075]
11. Niwa S, Tanaka Y, Hirokawa N. KIF1Bbeta- and KIF1A-mediated axonal transport of presynaptic regulator Rab3 occurs in a GTP-dependent manner through DENN/MADD. Nat Cell Biol. 2008; 10:1269–1279. [PubMed: 18849981]
12. Okada Y, Yamazaki H, Sekine-Aizawa Y, Hirokawa N. The neuron-specific kinesin superfamily protein KIF1A is a unique monomeric motor for anterograde axonal transport of synaptic vesicle precursors. Cell. 1995; 81:769–780. [PubMed: 7539720]
13. Pack-Chung E, Kurshan PT, Dickman DK, Schwarz TL. A Drosophila kinesin required for synaptic bouton formation and synaptic vesicle transport. Nat Neurosci. 2007; 10:980–989. [PubMed: 17643120]
14. Niwa S, Lipton DM, Morikawa M, Zhao C, Hirokawa N, Lu H, Shen K. Autoinhibition of a Neuronal Kinesin UNC-104/KIF1A Regulates the Size and Density of Synapses. Cell Rep. 2016; 16:2129–2141. [PubMed: 27524618]
15. Hammond JW, Cai D, Blasius TL, Li Z, Jiang Y, Jih GT, Meyhofer E, Verhey KJ. Mammalian Kinesin-3 motors are dimeric in vivo and move by processive motility upon release of autoinhibition. PLoS Biol. 2009; 7:e72. [PubMed: 19338388]
16. Wu YE, Huo L, Maeder CI, Feng W, Shen K. The balance between capture and dissociation of presynaptic proteins controls the spatial distribution of synapses. Neuron. 2013; 78:994–1011. [PubMed: 23727120]
17. Klassen MP, Wu YE, Maeder CI, Nakae I, Cueva JG, Lehrman EK, Tada M, Gengyo-Ando K, Wang GJ, Goodman M, et al. An Arf-like small G protein, ARL-8, promotes the axonal transport of presynaptic cargoes by suppressing vesicle aggregation. Neuron. 2010; 66:710–723. [PubMed: 20547129]

18. Hofmann I, Munro S. An N-terminally acetylated Arf-like GTPase is localised to lysosomes and affects their motility. J Cell Sci. 2006; 119:1494–1503. [PubMed: 16537643]
19. Kaniuk NA, Canadien V, Bagshaw RD, Bakowski M, Braun V, Landekic M, Mitra S, Huang J, Heo WD, Meyer T, et al. Salmonella exploits Arl8B-directed kinesin activity to promote endosome tubulation and cell-to-cell transfer. Cell Microbiol. 2011; 13:1812–1823. [PubMed: 21824248]
20. Pu J, Schindler C, Jia R, Jarnik M, Backlund P, Bonifacino JS. BORC, a multisubunit complex that regulates lysosome positioning. Dev Cell. 2015; 33:176–188. [PubMed: 25898167]
21. Starcevic M, Dell'Angelica EC. Identification of snapin and three novel proteins (BLOS1, BLOS2, and BLOS3/reduced pigmentation) as subunits of biogenesis of lysosome-related organelles complex-1 (BLOC-1). J Biol Chem. 2004; 279:28393–28401. [PubMed: 15102850]
22. Zheng Q, Ahlawat S, Schaefer A, Mahoney T, Koushika SP, Nonet ML. The vesicle protein SAM-4 regulates the processivity of synaptic vesicle transport. PLoS Genet. 2014; 10:e1004644. [PubMed: 25329901]
23. Klassen MP, Shen K. Wnt signaling positions neuromuscular connectivity by inhibiting synapse formation in C. elegans. Cell. 2007; 130:704–716. [PubMed: 17719547]
24. White JG, Southgate E, Thomson JN, Brenner S. The structure of the nervous system of the nematode Caenorhabditis elegans. Philos Trans R Soc Lond B Biol Sci. 1986; 314:1–340. [PubMed: 22462104]
25. Ou CY, Poon VY, Maeder CI, Watanabe S, Lehrman EK, Fu AK, Park M, Fu WY, Jorgensen EM, Ip NY, et al. Two cyclin-dependent kinase pathways are essential for polarized trafficking of presynaptic components. Cell. 2010; 141:846–858. [PubMed: 20510931]
26. Goody RS, Hofmann-Goody W. Exchange factors, effectors, GAPs and motor proteins: common thermodynamic and kinetic principles for different functions. Eur Biophys J. 2002; 31:268–274. [PubMed: 12122473]
27. Falcón-Pérez JM, Starcevic M, Gautam R, Dell'Angelica EC. BLOC-1, a novel complex containing the pallidin and muted proteins involved in the biogenesis of melanosomes and platelet-dense granules. J Biol Chem. 2002; 277:28191–28199. [PubMed: 12019270]
28. Di Giovanni J, Sheng ZH. Regulation of synaptic activity by snapin-mediated endolysosomal transport and sorting. EMBO J. 2015; 34:2059–2077. [PubMed: 26108535]
29. Cai Q, Lu L, Tian JH, Zhu YB, Qiao H, Sheng ZH. Snapin-regulated late endosomal transport is critical for efficient autophagy-lysosomal function in neurons. Neuron. 2010; 68:73–86. [PubMed: 20920792]
30. Zerial M, McBride H. Rab proteins as membrane organizers. Nat Rev Mol Cell Biol. 2001; 2:107–117. [PubMed: 11252952]
31. Gillingham AK, Munro S. The small G proteins of the Arf family and their regulators. Annu Rev Cell Dev Biol. 2007; 23:579–611. [PubMed: 17506703]
32. Guardia CM, Farías GG, Jia R, Pu J, Bonifacino JS. BORC Functions Upstream of Kinesins 1 and 3 to Coordinate Regional Movement of Lysosomes along Different Microtubule Tracks. Cell Rep. 2016; 17:1950–1961. [PubMed: 27851960]
33. Yonekawa Y, Harada A, Okada Y, Funakoshi T, Kanai Y, Takei Y, Terada S, Noda T, Hirokawa N. Defect in synaptic vesicle precursor transport and neuronal cell death in KIF1A motor protein-deficient mice. J Cell Biol. 1998; 141:431–441. [PubMed: 9548721]
34. Rosa-Ferreira C, Munro S. Arl8 and SKIP act together to link lysosomes to kinesin-1. Dev Cell. 2011; 21:1171–1178. [PubMed: 22172677]
35. Farías GG, Guardia CM, De Pace R, Britt DJ, Bonifacino JS. BORC/kinesin-1 ensemble drives polarized transport of lysosomes into the axon. Proc Natl Acad Sci U S A. 2017; 114:E2955–E2964. [PubMed: 28320970]
36. Zhao C, Takita J, Tanaka Y, Setou M, Nakagawa T, Takeda S, Yang HW, Terada S, Nakata T, Takei Y, et al. Charcot-Marie-Tooth disease type 2A caused by mutation in a microtubule motor KIF1Bbeta. Cell. 2001; 105:587–597. [PubMed: 11389829]
37. Mello C, Fire A. DNA transformation. Methods Cell Biol. 1995; 48:451–482. [PubMed: 8531738]
38. Arribere JA, Bell RT, Fu BX, Artiles KL, Hartman PS, Fire AZ. Efficient marker-free recovery of custom genetic modifications with CRISPR/Cas9 in Caenorhabditis elegans. Genetics. 2014; 198:837–846. [PubMed: 25161212]

39. Northup JK, Smigel MD, Gilman AG. The guanine nucleotide activating site of the regulatory component of adenylate cyclase. Identification by ligand binding. J Biol Chem. 1982; 257:11416–11423. [PubMed: 6288684]

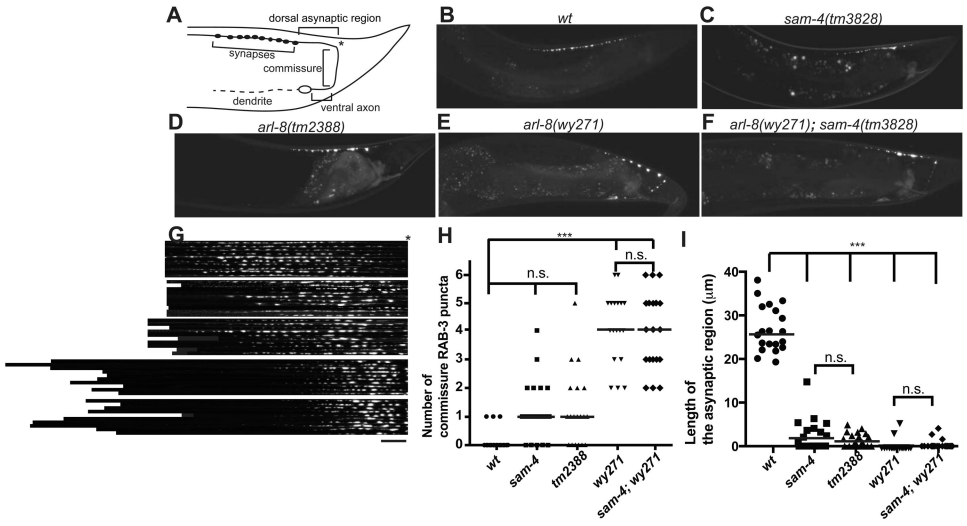

Figure 1. SAM-4 and ARL-8 are in the same pathway

(A) A schematic drawing of the DA9 neuron. The dorsal asynaptic region, the ventral axon and the commissure that are observed and analyzed in this study are shown. Asterisk indicates the location where the commissure joins the dorsal nerve cord.

(B-F) Representative images of GFP::RAB-3 in *wild type* (*wt)* (B), *sam-4(tm3828)* (C), *arl-8(tm2388)* (D), *arl-8(wy271)* (E) and *arl-8(wy271)*; *sam-4(tm3828)* (F). GFP::RAB-3 was expressed using the *itr-1 pB* promoter. Asterisks indicate the commissure bend shown in (A). Bars, 50 μm.

(G) Image montages of the dorsal axons in *wild type* (*wt)*, *sam-4(3828)*, *arl-8(tm2388)*, *arl-8(wy271)* and *sam-4(tm3828)*; *arl-8(wy271)*. 10 confocal images from each genotype were cropped, straightened and aligned in rows with the commissure bend (asterisk) on the right using Image J. Bar, 20 μm.

(H and I) Statistical analysis of mutant phenotypes. (H) The number of puncta mis-accumulated to the commissure and (I) the length of the asynaptic region. Lines show median values, and each dot represents one animal. Kruskal–Wallis one-way ANOVA on ranks and Dunn's multiple comparisons test; *Adjusted P Value < 0.05; **Adjusted P Value < 0.01; ***Adjusted P Value < 0.001. n= 20 animals for each genotype. See also Figure S1.

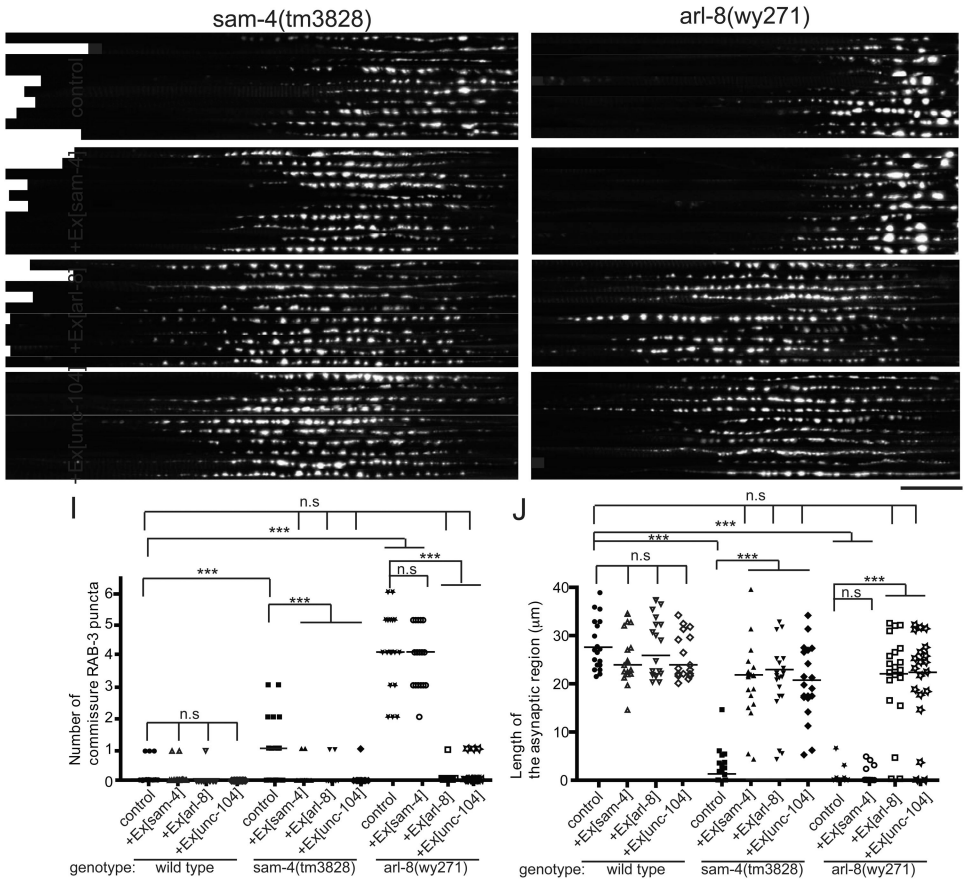

Figure 2. Hierarchal relation among *sam-4, arl-8* and *unc-104*

(A-H) Image montages of the dorsal axons in *sam-4(tm3828)* (A-D) and *arl-8(wy271)* (E-H) expressing *sam-4* cDNA (B and F), *arl-8* cDNA (C and G) and *unc-104* cDNA (D and H). *sam-4, arl-8* and *unc-104* cDNA were expressed using the *mig-13* promoter (DA9-specific promoter). Dorsal synapses were visualized using *Pitr-1::gfp::rab-3*. 10 confocal images from each genotype were cropped, straightened, and aligned using Image J. Representative results from at least three independent lines are shown. Bar, 20 μm.

(I and J) Statistical analysis of suppressor mutants. (I) The number of puncta mis-accumulated to the commissure and (J) the length of the asynaptic region. Lines show median values, and each dot represents one animal. Kruskal–Wallis one-way ANOVA on ranks and Dunn's multiple comparisons test; compared to wild type, *P Value < 0.05; **Adjusted P Value < 0.01; ***Adjusted P Value < 0.001. n= 20 animals for each genotype. See also Figure S2.

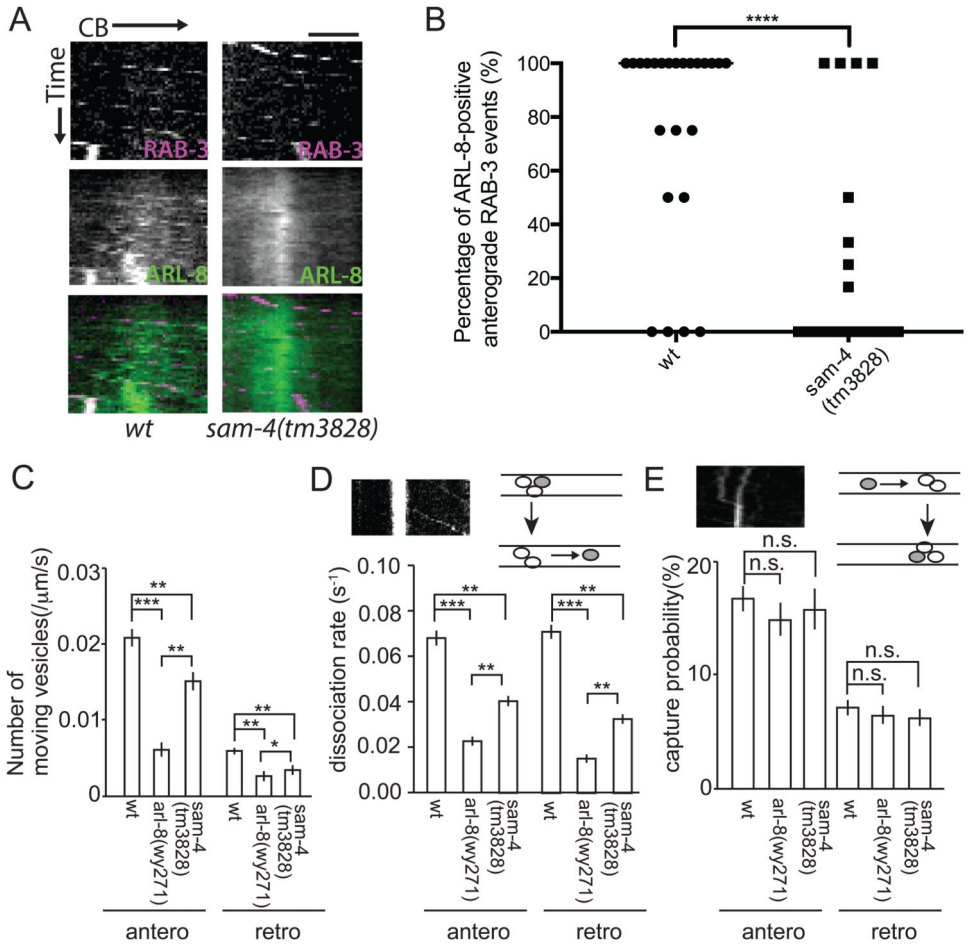

Figure 3. ARL-8 dynamics in the sam-4 mutant

(A) Representative ARL-8::YFP and mCherry::RAB-3 kymographs in the ventral axon of *wild type* (*wt*) and *sam-4(tm3828)* animals (*wyIs546*). Each dotted line represents one event; co-movement is visualized as staggering between dotted lines of different colors. ARL-8 co-migrates with SVPs marked by mCherry::RAB-3 in *wild type* (*wt*) but is detached from SVPs and largely diffused in *sam-4(tm3828)*. Scale bar represents 2.5 μm.

(B) Quantification of the percentage of ARL-8-positive anterograde RAB-3 events in *wild type* (*wt*) and *sam-4(tm3828)* animals. The percentage is calculated as the number of ARL-8-positive anterograde RAB-3 events over the total number of anterograde RAB-3 events. Lines denote median values, and each dot represents one animal. Mann-Whitney test; ****two-tailed P value<0.0001. n=24 and 25 animals for *wild type* and *sam-4(tm3828)*, respectively.

(C) Quantification of the number of moving vesicles in the proximal asynaptic region of axon, normalized to the duration and the length of the axon. n = 20 animals, t-test. ***p < 0.001, **p < 0.01 and *p < 0.05. Error bars represent SEM.

(D) Diagram and kymograph showing a dissociation event (arrow) and quantification of the dissociation rate at stable puncta in the proximal asynaptic region of axon axon. n = 20 animals. t-test. ***p < 0.001, **p < 0.01. Error bars represent SEM.

(E) Diagram and kymograph showing a mobile packet captured by a stable punctum(arrow) and quantification of the capture probability in the ventral axon. n = 20 stablepuncta. t-test; no statistical significance. Error bars represent SEM. See also Figure S3.

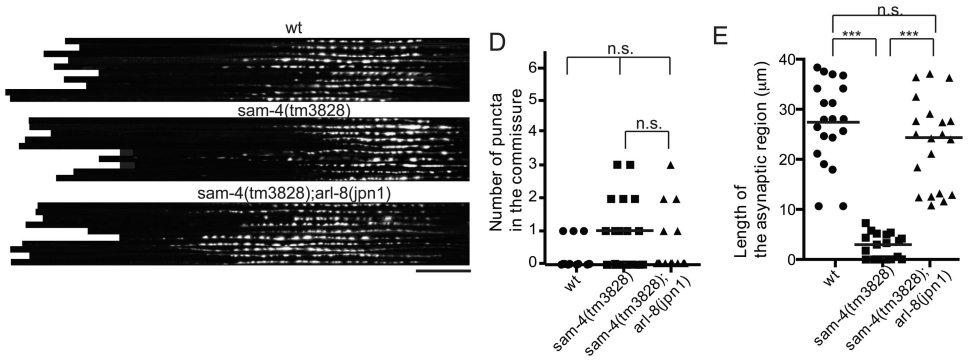

Figure 4. The *arl-8* mutation mimicking the GTP form suppresses *sam-4(tm3828)*

(A-C) Image montages of the dorsal axons in *wild type (wt)* (A), *sam-4(tm3828)* (B) and *sam-4(tm3828); arl-8(jpn1)* (C). Note that *arl-8(jpn1)* has a point mutation mimicking the GTP form. Dorsal synapses were visualized using *Pitr-1::gfp::rab-3*. 10 confocal images from each genotype were cropped, straightened and aligned at the commissure bend using Image J. Bar, 20 µm.

(D and E) The number of GFP: :RAB-3 puncta in the commissure (D) and the length of the asynaptic region (E). Lines show median values, and each dot represents one animal. Kruskal-Wallis one-way ANOVA on ranks and Dunn's multiple comparisons test; *Adjusted P Value < 0.05; **Adjusted P Value < 0.01; ***Adjusted P Value < 0.001. n= 20 animals for each genotype.

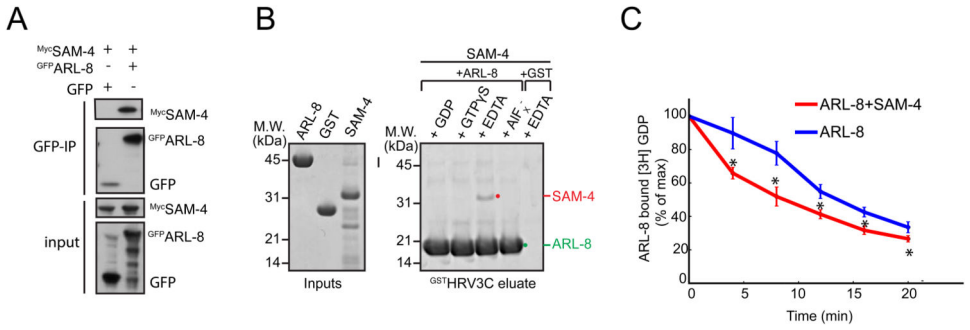

Figure 5. SAM-4 is a GEF for ARL-8

(A) Co-immunoprecipitation was performed with HEK293 cells that were transfected with GFP-tagged ARL-8 deleting the first 19 amino acids and Myc-tagged SAM-4 or GFP and Myc-tagged SAM-4.

(B)SAM-4 directly binds to ARL-8 in the present of EDTA. Purified SAM-4 was mixed with purified GST tagged ARL-8 or GST in the presence of GDP, GTPγ, GDP/AlF4− or EDTA, GST capture assay was performed using 10 μL Glutathione Sepharose beads, and eluted by HRV3C cleavage. Samples were analyzed by SDS page and Coomassie staining.

(C) SAM-4 accelerates [^{3}H]-GDP release from ARL-8. ARL-8 was preloaded with [^{3}H]-GDP and the remaining ARL-8 bound [^{3}H]-GDP was measured for 20 minutes. N = 3, mean ± SEM. *, $p < 0.05$, paired-t-test. See also Figure S4.

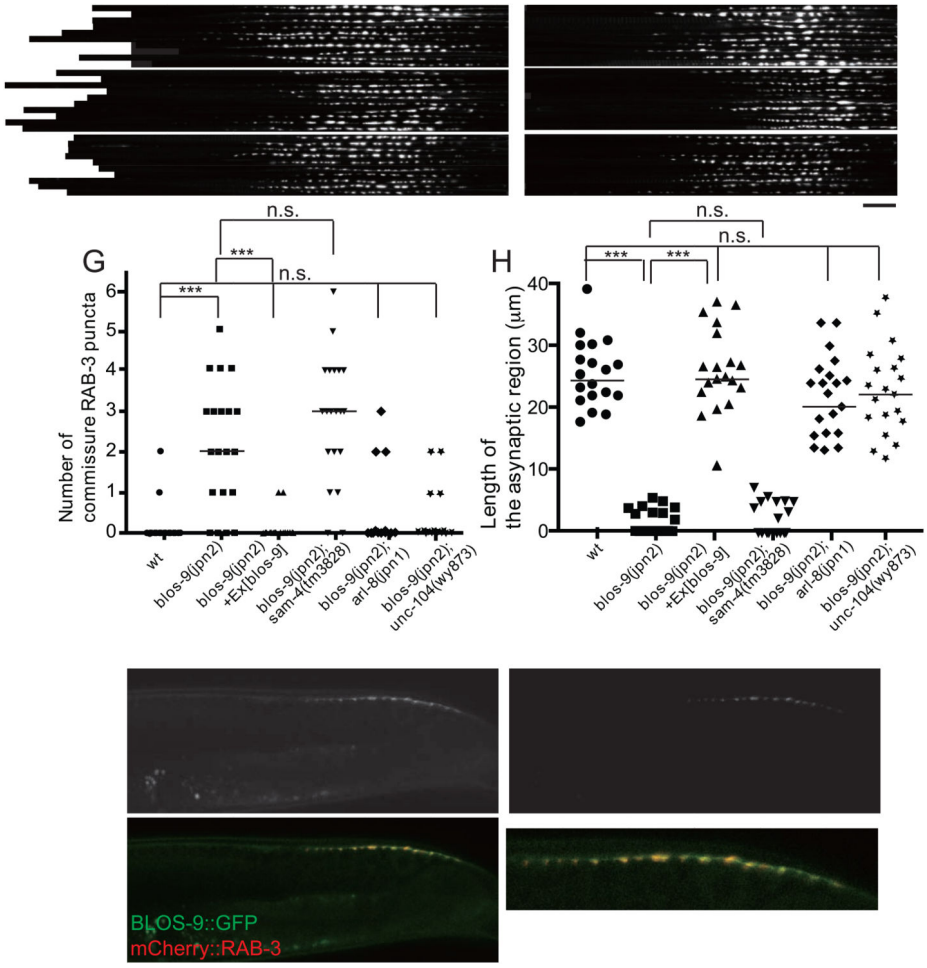

Figure 6. BLOS-9 regulates the axonal transport of SVs together with SAM-4

(A-F) Image montages of the dorsal axons in *wild type* (*wt*) (A), *blos-9(jpn2)* (B), *blos-9(jpn2)* expressing BLOS-9 using the DA9 promoter (C), *blos-9(jpn2)*; *sam-4(tm3828)* (D), *blos-9(jpn2)*; *arl-8(jpn1)* (E) and *blos-9(jpn2)*; *unc-104(wy873)* (F). Note that *arl-8(jpn1)* and *unc-104(wy873)* are gain-of-function alleles. Bar, 20 µm. (G and H) Statistical analysis of suppressor mutants. (G) The number of GFP::RAB-3 puncta mis-accumulated to the commissure and (H) the length of the asynaptic region. Lines show median values, and each dot represents one animal. Kruskal–Wallis one-way ANOVA on ranks and Dunn's multiple comparisons test; *Adjusted P Value < 0.05; **Adjusted P Value < 0.01; ***Adjusted P Value < 0.001. n= 20 animals for each genotype.

(I-L) The localization of (I) BLOS-9::GFP and (J) mCherry::RAB-3 in the dorsal synaptic region. The merged image is shown in (K). (L) A zoomed image of the boxed area in panel (K). BLOS-9 and RAB-3 are well co-localized. Bars, 50 µm. See also Figure S5.

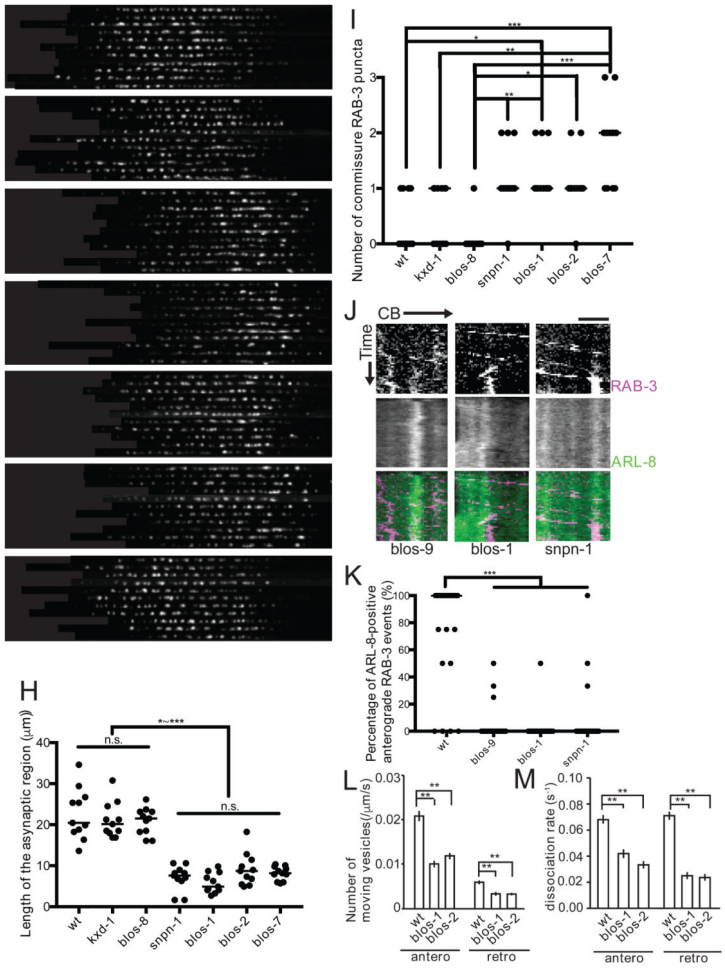

Figure 7. BORC subunits are essential for the axonal transport

(A-G) Image montages of GFP::RAB-3 in straightened DA9 dorsal axons, which are aligned at the commissure bend on the right and stacked in rows with one axon in each row, of *wild type* (*wt*) (A), *kxd-1(tm6384)* (B), *snpn-1(tm1892)* (C), *blos-1(ok3707)* (D), and *blos-2(jpn17)* (E), *blos-7(wy1159)* (F) and *blos-8(wy1160)* animals. Scale bar represents 5 μm.

(H) Quantification of the length of the asynaptic region in *wild type* (*wt*), *kxd-1(tm6384)*, *blos-8(wy1160)*, *snpn-1(tm1892)*, *blos-1(ok3707)*, *blos-2(jpn17)* and *blos-7(wy1159)* animals. The asynaptic region is defined as the distance between the commissure bend and the first bright GFP::RAB-3 punctum along the DA9 dorsal axon. Lines denote median values, and each dot represents one animal. Kruskal–Wallis one-way ANOVA on ranks and Dunn's multiple comparisons test; *Adjusted P Value < 0.05: *kxd-1* vs. *blos-2*, *blos-8* vs. *blos-2*; **Adjusted P Value < 0.01: *wt* vs. *blos-2*, *wt* vs. *blos-7*, *kxd-1* vs. *snpn-1*, *kxd-1* vs. *blos-7*, *blos-8* vs. *snpn-1*, *blos-8* vs. *blos-7*; ***Adjusted P Value < 0.001: *wt* vs. *snpn-1*, *wt* vs. *blos-1*, *kxd-1* vs. *blos-1*, *blos-8* vs. *blos-1*. n=11 animals for each genotype.

(I) Quantification of the number of GFP::RAB-3 puncta in the DA9 commissure in *wild type* (*wt*), *kxd-1(tm6384)*, *blos-8(wy1160)*, *snpn-1(tm1892)*, *blos-1(ok3707)*, *blos-2(jpn17)* and *blos-7(wy1159)* animals. Lines denote median values, and each dot represents one animal. Kruskal–Wallis one-way ANOVA on ranks and Dunn's multiple comparisons test; *Adjusted

P Value < 0.05; **Adjusted P Value < 0.01; ***Adjusted P Value < 0.001. n=11 animals for each genotype.

(J) Representative ARL-8::YFP and mCherry::RAB-3 kymographs in the ventral axon of *blos-9(jpn2)*, *blos-1(ok3707)*, and *snpn-1(tm1892)* animals (*wyIs546*). Each dotted line represents one event; co-movement is visualized as staggering between dotted lines of different colors. ARL-8 is detached from SVPs marked by mCherry::RAB-3 and largely diffused in the mutants. Scale bar represents 2.5 μm.

(K) Quantification of the percentage of ARL-8-positive anterograde RAB-3 events in *wild type* (*wt*), *blos-9(jpn2)*, *blos-1(ok3707)*, and *snpn-1(tm1892)* animals. The percentage is calculated as the number of ARL-8-positive anterograde RAB-3 events over the total number of anterograde RAB-3 events. Lines denote median values, and each dot represents one animal. Kruskal–Wallis one-way ANOVA on ranks and Dunn's multiple comparisons test; ***Adjusted P Value < 0.001. n=24, 22, 24, and 24 animals for wild-type, *blos-9(jpn2)*, *blos-1(ok3707)*, and *snpn-1(tm1892)*, respectively.

(L) Quantification of the number of events in the proximal asynaptic region of axon, normalized to duration and length of the axon. n = 20 animals, t-test. **p < 0.01. Error bars represent SEM.

(M) Quantification of the dissociation rate at stable puncta in the proximal asynaptic region of axon. Dissociation event is defined in Figure 3D. n = 20 animals. t-test. **p < 0.01. Error bars represent SEM. See also Figure S6 and S7.